Proceedings of the 10th Brazilian Congress of Thermal Sciences and Engineering -- ENCIT 2004
Braz. Soc. of Mechanical Sciences and Engineering -- ABCM, Rio de Janeiro, Brazil, Nov. 29 -- Dec. 03, 2004

Paper CIT04-0114

NUMERICAL COMPARISON OF THE COMBUSTION PROCESS INSIDE AN ALUMINUM MELTING FURNACE WITH NATURAL GAS AND LIQUID PENTANE

João N. E. Carneiro
Dept. Mechanical Eng, PUC/Rio, 22453-900, RJ, RJ, BRAZIL
carneiro@mec.puc-rio.br

Bruno Goes e Silva
Dept. Mechanical Eng, PUC/Rio, 22453-900, RJ, RJ, BRAZIL
bgoes@mec.puc-rio.br

Angela O. Nieckele
Dept. Mechanical Eng, PUC/Rio, 22453-900, RJ, RJ, BRAZIL
nieckele@mec.puc-rio.br

Mônica F. Naccache
Dept. Mechanical Eng, PUC/Rio, 22453-900, RJ, RJ, BRAZIL
naccache@mec.puc-rio.br

Marcos S. P. Gomes
Dept. Mechanical Eng, PUC/Rio, 22453-900, RJ, RJ, BRAZIL
mspgomes@mec.puc-rio.br

Abstract. *The choice of the type of fuel used as energy source for the aluminum melting can be of extreme importance for a better performance as well as for a greater preservation of the equipments. The option of a liquid or gaseous fuel can significantly alter the combustion aspects inside the furnace, such as the shape of the flame and the distribution of temperature and heat flux. In the present work, numerical simulations were carried out using the commercial package FLUENT, analyzing different cases with two types of fuel: a spray of liquid pentane and a natural gas jet, both reacting with pure oxygen. The results showed the possible damages caused by the process if long or too intense and concentrated flames are present, increasing very much the wall temperatures and compromising the heat flux on the aluminum surface.*

Keywords*. liquid Fuel, combustion, industrial furnaces*

1. Introduction

The experimental investigation of combustion processes is more difficult and expensive than numerical simulations. Thus, to evaluate the flow and heat transfer inside industrial equipment like furnaces or incinerators, and to perform a design optimization, the numerical simulation of the combustion process may prove to be a good alternative. Due to the complexity of the problem and great number of variables involved, a reliable analysis can only be possible with powerful numerical simulation software's.

In general, the use of liquid fuel is very common in the industry. However, the abundance of natural gas and the political need for developing a market in Brazil for this fuel, which can also very well meet the growing environmental restrictions, can motivate the substitution of fuel oils. It is, however, of fundamental importance to know if the operating characteristics of the equipments are maintained or even improved.

There are several works in the literature dedicated to the numerical investigation of combustion processes with different models. The Eddy Dissipation Concept (EDC) and the Probability Density Function (PDF) models were studied in the works of Gran and Magnussen (1996), Gran et al. (1997), Ma et al. (1999), and Magel et al. (1996). Correa and Shyy (1987) analyzed physical models and numerical techniques used in the simulation of pre-mixed turbulent gaseous combustion in complex geometries. It was observed that good results were obtained with finite rate models when the kinetic behavior was important. It was also noted that the κ–ε model was the most used turbulent model in numerical simulations. An interesting remark about the combustion model regards the need for simplicity, so that it may be realistically implemented in the solution codes. Gorner and Zinser (1990) presented the state-of-the-art in mathematical modeling of industrial flames and combustion chambers. They showed a simulation of a combustion process with multiple burners, for which it was obtained a good agreement between numerical and experimental results. Desjardin and Frankel (1996) presented a numerical simulation using the Linear Eddy Model, and compared it with the results of two other models: (1) the Stationary Laminar Flamelet Model, and (2) the Conditional Moment Closure Method. Gomes et al. (1997) compared numerical results carried out with the generalized finite rate method with experimental data, obtaining a good qualitative agreement. Zimont et al. (1998) described the theory, implementation and results when using a computational model, which simulates the turbulent combustion of pre-mixed gases with high Reynolds numbers. Their results were in

agreement with experimental data, indicating that the model could be very useful for dealing with the simulations of complex geometries. Christo et al. (1998) employed different turbulence and combustion models in the simulation of a landfill-gas flare. The authors discussed about the limitations of the Eddy-break-up model. The numerical results also showed good agreement with the experimental data. Goldin and Menon (1998) showed a comparison between various PDF turbulent combustion models in non-premixed turbulent jet flames. They investigated the performance of a conventional PDF model against a proposed model, in which the solution of the chemical kinetics was decoupled from the solution of the momentum equation. Eaton et al. (1999) provided an overview of the combustion modeling technology applied to fossil-fuel combustion, and showed some comparisons between numerical results and experimental data. Nieckele et al (1998, 1999, 2004) analyzed the flow field inside aluminum furnaces with different types of burners and operating conditions. Brewster et al (2001) investigated numerically and experimentally an industrial aluminum melting furnace with oxygen enriched combustion. The temperature distribution on the refractory walls was verified. The model over estimated the turbulent mixture and, on the other hand, the CO (carbon monoxide) concentrations were under estimated near the burner region, probably because the kinetic effects were neglected. Numerical simulations inside an industrial burner in an aluminum melting furnace were also carried out by Mukhopadhyay et al (2001). They showed that the flame height grows with the fuel velocity for a given air-fuel ratio, and with the reduction of the air velocity, for a given fuel velocity. Nieckele et al (2002) simulated a turbulent natural gas flame in a cilindrical furnace, using finite rate models and modeling chemical reactions in two different ways: in a simple manner, where the fuel combustion was predicted in one single global reaction; and with a two-step process, where the carbon monoxide could be predicted in an intermediate reaction. The results for both models showed a good agreement with the experimental data found in the literature, although it was observed that the physical phenomena was better described by the two step reaction.

With respect to the numerical modeling of the spray flow of liquid fuels, Jones et al (2000) proposed a stochastic modeling for the turbulent dispersion of the spray droplets. The approximation adopted led to plausible results when applied to a kerosene spray flame, being therefore considered a good method for predicting the liquid film break-up and the process of droplet formation. Reveillon et al (2000) modeled numerically the vaporization of liquid fuel sprays in a turbulent non-premixed flame, proposing a single model that predicted the source terms for the mean mixture fraction and ts variance. The source term for the mean mixture fraction due to the droplet vaporization is normally provided by an Eulerian-Lagrangean formulation which, according to the authors, is not satisfactory when applied to the calculation of the source terms that are associated to the fluctuations of the mixture fraction. Demoulin et al (2002) investigated numerically the turbulent combustion of a liquid fuel spray, and utilizing probability density functions for each fluctuating variable in the liquid and gas phases, showed that a correct description of the temperature fluctuations caused by the presence of the droplets in the flow field is crucial for a better estimation of the reaction rates.

The purpose of the present work is the comparison of the combustion process inside an aluminum melting furnace, using two different types of fuel with similar heating power: natural gas and liquid pentane.

The turbulent flow and heat transfer analyses were carried out using the commercial software FLUENT, V6.1. The governing conservation equations for mass, momentum, energy and n-1 species were solved via a finite volume formulation. To simulate the combustion process the generalized finite rate model was employed, with a combined Arrhenius-Magnussen reaction rate expression. High temperatures due to the combustion reactions require the modeling of a radiation source term for the energy equation. For the turbulence phenomena, the two differential equation $\kappa-\varepsilon$ model was chosen. An additional model is necessary to describe the coupling between the continuous and discrete phases (pentane droplets) of the liquid fuel.

2. Problem set-up

The geometry corresponds to that of a simplified furnace, which was represented as a rectangular prism of 4.0m length, 1.5m wide and 2.0m height. A schematic diagram of the geometry with the coordinate system is presented in Fig. 1, while Fig. 2 illustrates details of the frontal plane, and different view of the inlet configuration.

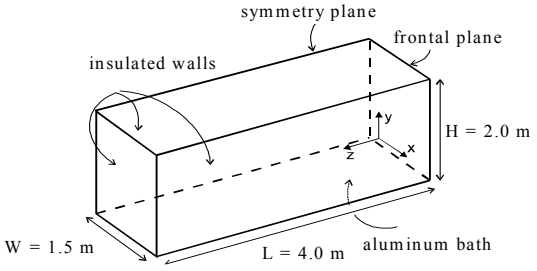

Figure 1– Schematic of the furnace and geometry

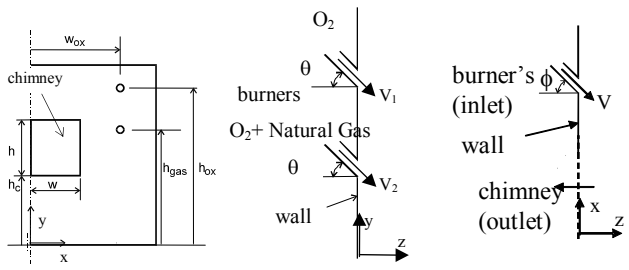

Figure 2– Injection and chimney geometry:

The lower limit of the furnace was considered to be the liquid aluminum surface with a small aluminum oxide layer of 5 mm above it. The aluminum oxide layer was considered to describe the oxidization of the aluminum surface by the water that results from the combustion, which can act as an isolator and can compromise the quality of the product.

The vertical symmetry plane passes through the center of the chimney between the two pairs of oxygen and fuel injectors. The inlets of oxygen and fuel as well as the outlet of the combustion products are located at the same wall (Fig. 2). The center of the burner is located 0.65m above the aluminum oxide layer and 0.80m away from the symmetry plane, with an internal diameter of 0.0192m (fuel injection) and external radius of 0.0096m (oxygen injection through the annular gap, surrounding the fuel jet). The oxygen injector is located 0.20m above the burner, with the same dimensions. So that the jets are directed away from the refractory walls, angles of 15° in the vertical plane and 10° in the horizontal plane were set. The height of the center of the rectangular chimney coincides with that for center of the burner, its half width measures 0.50m and its height measures 0.60m.

The furnace has a nominal thermal power of 1.25 MW per burner (2.5 MW total). Considering a typical aluminum load of 16 tons (which corresponds to a volume of $6m^3$ and a latent heat of 397.4 kJ/kg) and an approximate process time of 1 hour, a negative heat sink of 1.77 MW (71% of the total) was prescribed, in order to represent both the energy necessary to melt the entire load of aluminum and the possible heat losses inherent in the process.

Two cases were analyzed (half furnace, due to the geometry symmetry), concerning the gas and liquid fuels: the first one with a 1.25 MW natural gas (h_{ci} = 44800 kJ/kg) flame, and the second one with a 1.25 MW pentane (h_{ci} = 38345 kJ/kg) flame. The mass flow rates were, therefore, for the gas and liquid fuel, 3.47×10^{-2} kg/s and 2.97×10^{-2} kg/s. Considering the specific mass of the pentane and natural gas as 620 kg/m^3 and 0.795 kg/m^3 (at 1 atm and 25 C) respectively, and an inlet cross section of 2.89×10^{-8} m^2 (central orifice), the magnitude of the inlet fuel velocities were 159 m/s and 0.175 m/s,. The oxygen-fuel ratio was stoichiometrically defined for both cases. The total oxygen mass flow rate was equally divided into each inlet. Considering its specific mass of 1.3 kg/m^3 and the natural gas composition, oxygen was injected at 260 Nm^3/h for the first case, and for the pentane case at 0.106 kg/s.

The composition considered for the natural gas, the molecular weight of the species, M_i, the formation enthalpy h_i^o (reference temperature of 298 K) and the specific heat cp_i are presented in the table below (Van Wylen, 1976, and Kuo, 1986):

Table 1 – Natural gas properties

Species	**% m_i**	**M_i**	**h_i^o [kJ/kg]**	**cp_i [J/(kg K)]**
CH_4	70.3	16	-74 895	2 222
C_2H_6	17.8	30	-83 863	1 731
C_3H_8	0.69	44	-103 860	1 549
CO	0.00	28	-110 530	1 043
CO_2	6.93	44	-39 353	840
N_2	4.28	28	0.0	1 041
H_2O	0.00	18	-241 830	2 014
O_2	0.00	32	0.0	919

The following thermophysical properties were considered. The absolute viscosity and thermal conductivity were set equal to μ= 1.72×10^{-5} Pa s. and k= 0.0241 W/(m K). The diffusion coefficient of all species in the mixture was equal to the N_2 diffusion coefficient, 2.88×10^{-5} m^2/s. The species' specific heat at constant pressure were obtained as a function of temperature, and the mixture specific heat was obtained by a weighted mass fraction average.

To model the pentane spray concerning the liquid fuel problem, 15 inlet points were uniformly distributed into the fuel inlet region. The droplets flow is defined from initial conditions related to the injection points of the discrete phase in the gaseous mixture. These conditions will be used as the start point for the integration of the droplets equation of motion and calculation of their trajectories. Since the surface combustion of the particle is not being modeled, the droplets must vaporize to react with the gaseous phase. Therefore, the inlet temperature of the droplets influences the point where the combustion reaction will start. The vaporization temperature was defined as the same temperature at which the droplets enter the domain (303 K), indicating that vaporization starts immediately after they are inside the furnace, that is, no inert heating occurs. Unless the particle temperature has reached the boiling point, the vaporization is controlled by the fuel vapor pressure (defined as 8.2×10^4 Pa) and by the droplets diffusion coefficient (6.1×10^{-6} m^2/s). If the boiling temperature is reached, the boiling rate equation (eq. (23)) is used to predict the convective boiling of a discrete phase droplet. In that case, the rate of phase change of the liquid fuel is extremely dependent on its latent heat (3.63×10^5 J/kg).

2. Model description

For simulating the turbulent flow within the furnace, the time average forms of the continuity and linear momentum equations were solved via the finite volume technique, with the commercial code FLUENT, version 6.1. The Boussinesq's hypothesis was adopted, leading to an effective viscosity μ_{ef}. Therefore, the continuity and momentum equations are given by:

$$\mathbf{div}\,(\rho\ \mathbf{v}) = 0 \qquad (1)$$

$$\mathbf{div}(\rho \mathbf{v}\mathbf{v}) = \mathbf{div}[\mu_{ef}\ (\mathbf{grad}\ \mathbf{v} + (\mathbf{grad}\ \mathbf{v})^{T})] + \rho \mathbf{g} - \mathbf{grad}\ P \tag{2}$$

$$\mu_{ef} = \mu + \mu_t \qquad ; \qquad \mu_t = (c_\mu\ \rho \kappa^2)/\varepsilon \tag{3}$$

$$P = p - (2/3)[\mu_{ef}\ \mathbf{div}\ \mathbf{v} + \rho\kappa] \tag{4}$$

where **v** is the velocity vector, ρ is the specific mass, **g** is the gravity vector, P is a modified pressure, μ_{ef}, μ and μ_t are the effective, absolute viscosity and turbulent viscosity, respectively. The turbulent viscosity μ_t was obtained by the κ–ε turbulence model. This model has been extensively employed along the years in the simulation of turbulent flow. In this model, the turbulent viscosity may be expressed in terms of the turbulence kinetic energy κ and the dissipation for the turbulence kinetic energy ε, according to Eq. 3. Equations (5) and (6) represent the conservation of κ and ε respectively, where the term G stands for the generation of turbulence kinetic energy.

$$\mathbf{div}(\rho \mathbf{v}\kappa) = \mathbf{div}\left[(\mu_t/Pr_\kappa)\ \mathbf{grad}\ \kappa\right] + (G - \rho\ \varepsilon) \tag{5}$$

$$\mathbf{div}\ (\rho\ \mathbf{v}\ \varepsilon) = \mathbf{div}\left[(\mu_t/Pr_\varepsilon)\ \mathbf{grad}\ \varepsilon\right] + (c_1\ G - c_2\ \rho\ \varepsilon)\ (\varepsilon/\kappa) \tag{6}$$

$$G = \mu_t \left[\text{grad}\ \mathbf{v} + (\text{grad}\ \mathbf{v})^T\right] \circ \text{grad}\ \mathbf{v} \tag{7}$$

The above equations were solved simultaneously with the equations of continuity and conservation of momentum, providing the solution for the turbulent flow problem. The constants used in the κ–ε model were c_1=1.4, c_2=1.9, and c_μ=0.09. The turbulent Prandtl for κ and ε were set equal to 0.7. The density of the gaseous mixture was calculated using the ideal gas law, $\rho = p_{op}/[RT\ \Sigma_i\ (m_i/M_i)]$, where p_{op}=1 atm is the average operation pressure inside the furnace.

For all dependent variables, wall functions were employed for setting up the conditions close to the solid boundaries, following the procedure described in Patankar and Spalding (1967) and in Launder and Spalding (1974).

The enthalpy within the furnace was obtained solving the energy equation:

$$\mathbf{div}\ (\rho\ \mathbf{v}\ h) = \mathbf{div}\left[(\mu/Pr + \mu_t/Pr_t)\ \mathbf{grad}\ h\right] + \mathbf{v} \bullet \mathbf{grad}\ p + S_h \tag{8}$$

where the total enthalpy h is defined by the sum of the enthalpies for each species h_i weighted by its mass fraction m_i, $h = \Sigma_i\ m_i\ h_i$. The term $S_h = S_{reac} + S_{rad}$, represents the enthalpy source due to the chemical reactions (combustion) and the radiation heat transfer. The turbulent Prandtl number, Pr_t, was set at 0.5. The temperature can be obtained from the enthalpy by

$$h^* = \sum_j m_j \left[\int_{T_{ref}}^{T} cp_j\ dT + \frac{h_j^o}{M_j} + \int_{T_{ref\,j}}^{T_{ref}} cp_j\ dT \right] \tag{9}$$

where cp_j is the specific heat at constant pressure, M_j is the molecular weight, T is the temperature, m_j is the mass fraction and h_j^o is the formation enthalpy. The subscript j refers to each species.

Due to the high temperatures found inside the furnace, it is necessary to account for the radiation heat transfer, and the Discrete Transfer Radiation Model (DTRM) was selected. In this model, the change in the radiant intensity I, integrated over all wavelengths, along a path S is calculated according to $dI/dS = -\alpha I + \alpha \sigma T^4/\pi$, if scattering is neglected. The terms on the right side represent the loss by absorption and the gain by emission due to the participating medium, respectively (Siegel and Howell, 1981). The radiant intensity is obtained by the integration along several directions starting from each control volume on the domain surfaces. The source for enthalpy due to radiation heat transfer R_{rad} is calculated locally by summing the changes in intensity for all the rays crossing the control volume. The Weighted Sum of Gray Gases Model (WSGGM) was used for the calculation of the absorption coefficient, (Fluent User's Guide, 1995; Smith *et al.*, 1982).

To model the combustion process, the generalized finite rate model with three different reaction rates was employed. In this model, the chemical species distributions are determined through the solution of their transport conservation equations. The gas phase transport was calculated solving a set of *n-1* conservation equations for chemical species, where *n* represents the number of species. The general form of the conservation equation for each chemical species m_i is given by:

$$\mathbf{div}\ (\rho\ \mathbf{v}\ m_i) = \mathbf{div}\left[(\mu/Sc + \mu_t/Sc_t)\ \mathbf{grad}\ m_i\right] + R_i + S_i \tag{10}$$

where R_i and S_i represent the sources for each species. The former is associated with the transformations due to chemical reactions, and is expressed as the sum of the reaction rates (generation or consumption) for species i in every reaction k, $R_{i,k}$, so that $R_i = \Sigma_k R_{i,k}$. The source S_i comes from the dispersed phase. Turbulence is taken into account via the turbulent diffusion coefficient, μ_t/Sc_t, where the turbulent Schmidt number Sc_t was set equal to 0.5. The rates in the combustion reactions were calculated by using three models: the Arrhenius model, the Magnussen model and the combined Arrhenius-Magnussen model (Kuo, 1986; Fluent User's Guide 1995).

In the Arrhenius model, the reaction rate may be computed according to

$$R_{i,k} = \eta_{i,k} M_i T^{\beta_k} A_k \exp\left(-E_k / RT\right) \prod_j C_j^{\gamma_{j,k}} \tag{11}$$

where η_i is the stoichiometric coefficient, M_i is the molecular weight and C_i is the molar concentration of specie i, A_k is pre-exponential factor and E_k is the activation energy of reaction k, R is the gas constant, β_k is the temperature exponent and $\gamma_{i,k}$ is the concentration exponent of specie i in reaction k.

.In the Magnussen model, the reaction rate is calculated taking the lowest value of the following equations

$$R_{i,k} = \eta_{i,k} M_i K_1 \rho \frac{\varepsilon}{k} \frac{m_{j*}}{\eta_{j*,k} M_{j*}} \tag{12}$$

$$R_{i,k} = \eta_{i,k} M_i K_1 K_2 \rho \frac{\varepsilon}{k} \frac{\sum_p m_p}{\sum_p \eta_{p,k} M_p} \tag{13}$$

In these expressions $j*$ represents the reactant that gives the lowest value for $R_{i,k}$, and K_1 and K_2 are empirical constants, set as 4.0 and 0.5, respectively.

Finally, as recommended by Fluent (1995), for the combined Arrhenius-Magnussen model, the final value for the reaction rate is the lowest value between the ones obtained with the Arrhenius and the Magnussen models, so that for low value of κ, laminar regime, the Arrhenius expression is employed.

The prediction of the trajectory of a discrete phase droplet is performed by integrating the force balance on the droplet, which is written in a Lagrangian reference frame as follows:

$$\frac{d u_p}{d t} = F_D(u - u_p) + g_x(\rho_p - \rho)/\rho_p \tag{14}$$

$$F_D(u - u_p) = (18\,\mu)/(\rho_p\, d_p^2)\, C_D\, \mathbf{Re}_p / 24 \tag{15}$$

$$\mathbf{Re}_d = \rho\, d_p \left| u_p - u \right| / \mu \tag{16}$$

where $F_D(u - u_p)$ is the drag force per unit particle mass and $\mathbf{Re}_d$ is the relative Reynolds number, u and u_p are the fluid phase and particle velocities, and d_p is the particle diameter. C_D is the drag coefficient, which depends on $\mathbf{Re}_d$

As the trajectory of a particle is computed, the droplet stream variation of heat, momentum and mass are incorporated in the subsequent continuous phase calculations. By doing so, the interphase exchange is alternately computed, considering the droplets trajectories and the conservation equation for the gaseous mixture, until the solutions in both phases stop to change.

There are basically two mechanisms that control the droplets evaporation, depending on its temperature level, T_p. If the temperature is higher then T_{bp} (boiling point) the boiling process is convective, and no longer controlled by the diffusion of molecules on the droplets surface to the continuous phase and the fuel vapor pressure. Therefore, for $T_p < T_{bp}$

$$N_i = k_c\,(C_{i,s} - C_{i,\infty}) \tag{17}$$

where N_i is the vapor molar flux, k_c is the mass transfer coefficient, $C_{i,s}$ and C_i, are the concentrations on the droplets surface and in the gaseous phase, respectively. For $T_p \geq T_{bp}$:

$$\frac{d d_p}{dt} = \frac{4 k_\infty}{\rho_p c_{p,\infty} D_p} (1 + 0{,}23\sqrt{\mathbf{Re}_d}) \ln\left[1 + \frac{c_{p,\infty}(T_\infty - T_p)}{h_{fg}}\right] \tag{18}$$

where $c_{p,\infty}$, k_∞ and T_∞ are, respectively, the specific heat at constant pressure, thermal conductivity and gas temperature, and $h_{f,g}$ is the latent heat of volatiles involved.

The coupling between the discrete and continuous phases appears as source terms in the momentum, energy and mass equations for the continuous phase. The drag force acting on the droplet in axial direction depends on the mass flow rate of the droplet, $\dot{m}_p$. It is integrated in time with a time step Δt.

$$F = \sum \frac{18\,\mu\, C_D\, \mathbf{Re}_d}{\rho_p d_p^2\, 24}(u_p - u)\,\dot{m}_p \Delta t \tag{19}$$

Neglecting the presence of superficial combustion, the energy exchange between phases is calculated by:

$$Q = \left[\frac{\overline{m}_p}{m_{p,o}} c_p\, \Delta T_p + \frac{\Delta m_p}{m_{p,o}} \left(-h_{f,g} + h_{pyrol} + \int_{T_{ref}}^{T_p} c_{p,i}\, dt \right) \right] \dot{m}_{p,o} \tag{20}$$

where $\overline{m}_p$ is the average mass of the droplet in the control volume, $m_{p,o}$ and c_p are the initial mass and specific heat of the droplet, ΔT_p and Δm_p are temperature and mass variation as the droplet passes through the control volume, $h_{f,g}$ is the latent heat of the volatiles involved, h_{pyrol} and $c_{o,i}$ are the heat of pyrolisis and specific heat of theses volatiles, T_p is the droplet temperature on the control volume exit, T_{ref} is the enthalpy reference temperature.

The mass transfer to the continuous phase is calculated by examining the mass change of the droplet as it passes through each control volume:

$$M = (\Delta m_p / m_{p,o})\,\dot{m}_{p,o} \ . \tag{21}$$

2.1. Reactions

Two cases were considered. Natural gas was employed for the first case, while for the second case, the simulation was carried on with pentane as the liquid fuel. A five step mechanism was selected for Case 1, and a simple mechanism of one step was implemented for Case 2, as shown in Table 2.

Table 2 – Reactions

	Case 1 – Natural Gas	Case 2 – Liquid Fuel
Reaction		
1	$CH_4 + 3/2\ O_2 \rightarrow CO + 2\ H_2O$	$C_5H_{12} + 8\ O_2 \rightarrow 5\ CO_2 + 6\ H_2O$
2	$CO + 1/2\ O_2 \rightarrow CO_2$	
3	$C_2H_6 + 5/2\ O_2 \rightarrow 2\ CO + 3\ H_2O$	
4	$C_3H_8 + 7/2\ O_2 \rightarrow 3\ CO + 4\ H_2O$	

The stoichiometric coefficients for each reaction must be specified in accordance to equations in Table 2. The Magnussen reaction rate expression does not require any additional information. The parameters for Arrhenius and Arrhenius-Magnussen models are shown in Tables 3 and 4, where β_k was set as zero for all reactions.

Table 3 – Parameters for each reaction for the Arrhenius reaction rate expression, Eq. (10) – Case 1

Reaction	A_k(m^3/s)/kmol	E_k J/kmol	γ_{CH4}	γ_{C2H6}	γ_{C3H8}	γ_{O2}	γ_{CO2}	γ_{CO}	γ_{H2O}
1	5.01×10^{11}	2.00×10^{8}	0.7	-	-	0.8	-	0	0
2	6.19×10^{9}	1.26×10^{8}	-	0.1	-	1.65	0	-	0
3	5.62×10^{9}	1.26×10^{8}	-	-	0.1	1.65	-	0	0
4	2.24×10^{12}	1.70×10^{8}	-	-	-	0.25	0	-	-

Table 4 – Parameters for each reaction for the Arrhenius reaction rate expression, Eq. (10) – Case 2

Reaction	A_k(m^3/s)/kmol	E_k J/kmol	β_k	γ_{C2H5}	γ_{O2}	γ_{CO2}	γ_{H2O}
1	3.60×10^{9}	1.26×10^{8}	0	0.25	1.5	0	0

3. Results

The flow field inside the furnace was numerically obtained with FLUENT for the two types of fuel. The solution was considered converged when the sum of the normalised residuals of all equations was less than 10^{-4} and the normalised enthalpy residual was less than 10^{-6}.

After a mesh test, an approximately uniform mesh of 371250 (55×82×90) control volumes was generated with the FLUENT auxiliary tool GAMBIT (Fluent, 2002). Figure 3 illustrates the mesh distribution.

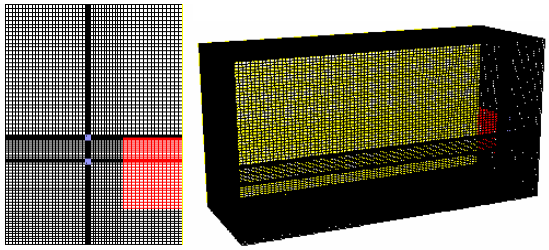

Figure 3– Mesh distribution

3.1. Temperature and heat flux distribution

Figures 4 and 5 present isosurfaces of temperature both fuel. Figure 4 corresponds to T= 2000K, while at Fig. 5, T=3000 K. Both flames follow the direction of the inlet jets, away from the refractory walls and downward into the load's surface. At Fig. 4a, a long isosurface can be seen for Case 1, while a very small isosurface of T=3000K can be seen in Fig. 5a. For Case 1, the combustion starts near the entrance, where very high values are then obtained, and rapidly the temperature level drops to 2000K. For Case 1, the temperature level inside the furnace is approximately 1500K. The same behavior is not seen for the pentane. At Fig. 4b, two small isosurface equal to T=2000 K can be seen near the burner. At Fig. 5b, a larger region around them, corresponding to a warmer isosurface, T=3000K, can be seen. The pentane flame appears to be displaced from the inlet, which can be explained by the fact that the droplets must first vaporize and to be absorbed by the gaseous mixture to react with the oxygen. For Case 2, the temperature level inside the furnace is much higher, approximately 2500K.

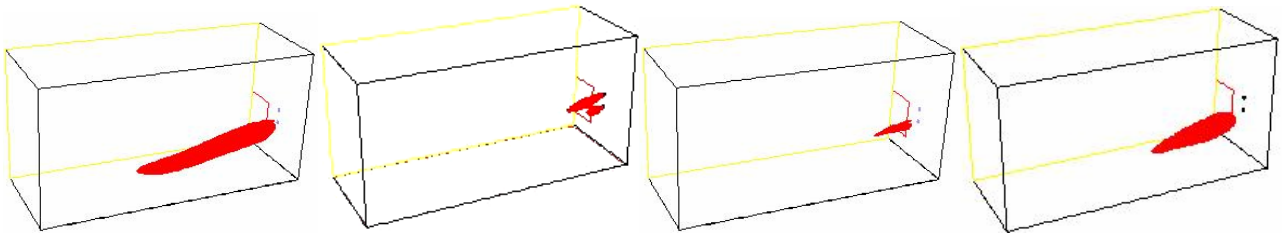

(a) natural gas (b) pentane

Figure 4 – Isosurfaces of temperature, T=2000K

(a) natural gas (b) pentane

Figure 5– Isosurfaces of temperature, T=3000K

The purpose of the comparison is to show different shapes of the flame associated to different types of fuel and its combustion aspects. While the gas flame extends itself through the furnace, the pentane flame is more intense and concentrated in the first third of the domain. That leads to a less uniform temperature distribution on the refractory walls (shown in Fig. 6) and could also compromise the uniformity of the heat flux on the aluminum surface. At Figure 6, the influence of the flame at the refractory wall is clearly seen in both cases, by the warm spots at the side wall. These warm spots can damage the refractory wall, increasing the cost of the project. Although qualitatively the temperature distribution is similar for both cases, the temperature level inside the furnace is much higher with the pentane than with natural gas, as already mentioned.

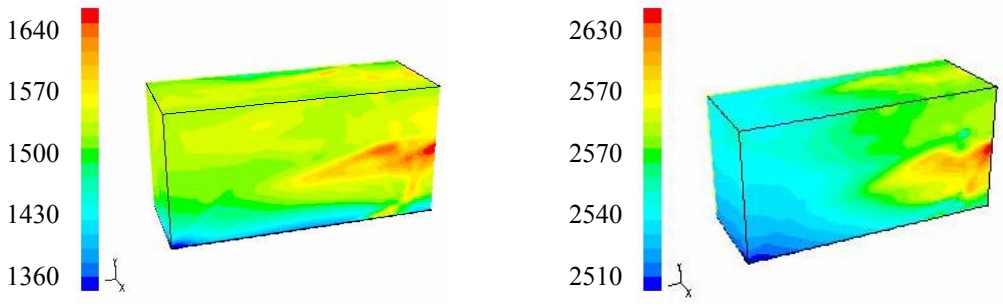

(a) natural gas (b) pentane

Figure 6 – Temperature distribution on the refractory walls.

The radiation heat flux on the aluminum surface is presented at Fig. 7. At this figure the isosurface representing the flame is also shown. Due to the high temperature flame, the radiation heat flux is dominant. It can be seen large values of the radiation heat flux under the flame for both cases. Since the pentane flame was much more concentrated, a less uniform heat flux was obtained in this case.

Figure 8 shows the temperature distribution on a plane that passes through the injectors (x = 0.80m). In both cases, it can be seen the cold oxygen jet over the pentane spray and natural gas jet, close to the inlet region. Due to the combustion, a substantial temperature raise can be observed in both cases. The high temperature region can be interpreted as the flame region. Thus, it can be seen, that the flame region is closer to the entrance for the natural gas case than it is for the pentane case. It is also observed that the temperature level inside the furnace is higher for the liquid fuel than for the natural gas combustion.

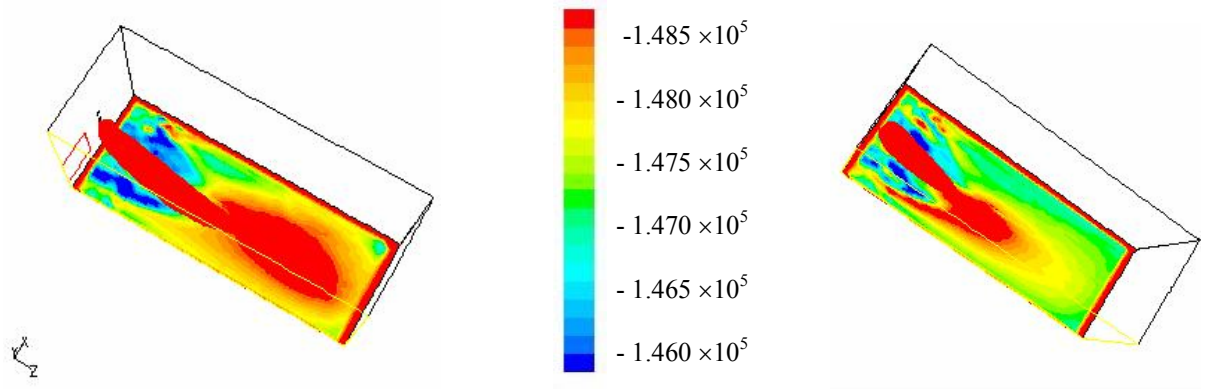

(a) natural gas (b) pentane

Figure 7 – Distribution of radiation heat flux (W/m^2)

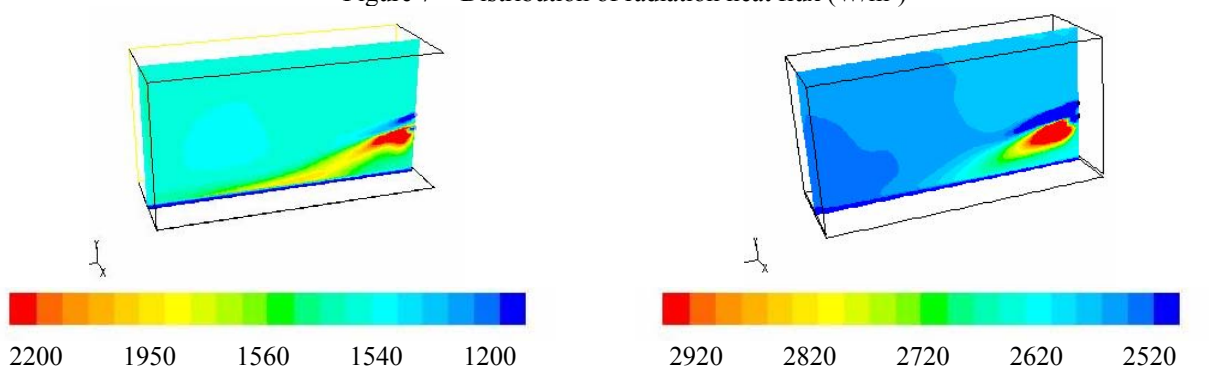

(a) natural gas (b) pentane

Figure 8 – Temperature (K) distribution. Plane y-z (x=0.8 m)

Figure 9 shows the temperature profile along the *z* coordinate for two lines inside the furnace. The first line passes through the center of the burner (x = 0.80m and y = 0.65m), and another one passes through the center of the oxygen injector (x = 0.80m and y = 0.85m). It can be seen that, as already mentioned, the temperature levels inside the furnace were higher for the liquid fuel than for the natural gas. After the flame region, the temperature of the liquid fuel (2600 K), is approximately 1000 K higher for the natural gas (2600 K), although the natural gas peak temperature reaches this level in the line passing through the center of the burner. There is a depression on the temperature level at y=0.65 m for both cases. This is due to the fact that the inlet fuel/oxygen are cold, and only after both species are brought to contact, the combustion process starts. Since there is only oxygen in the lower entrance, it reduces the temperature of the warmer mixture that arrives from the upper burner.

Figure 10 presents contours of temperature on the outlet of the combustion products (chimney) for both cases, and a detail of the flame. It can be clearly seen that the flame is detached from the burner for the liquid fuel case, since the combustion only starts after the liquid drops have vaporized. It can also be seen at this figure the presence of undesirable hot spots on the chimney corners.

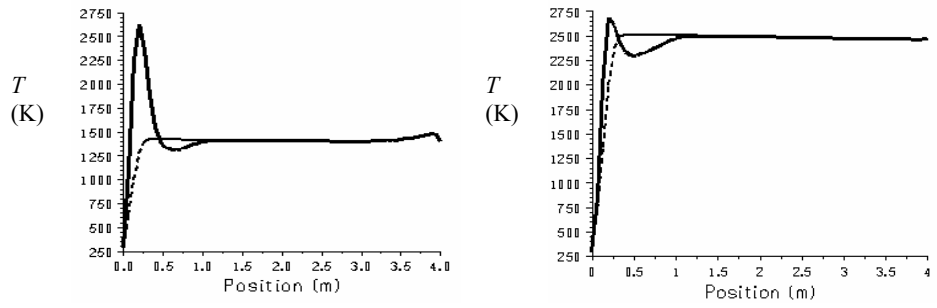

(a) natural gas (b) pentane

Figure 9 – Temperature profiles along lines inside the furnace. z variation, x = 0.80 m; y = ___0.65 e - - - - 0.85 m.

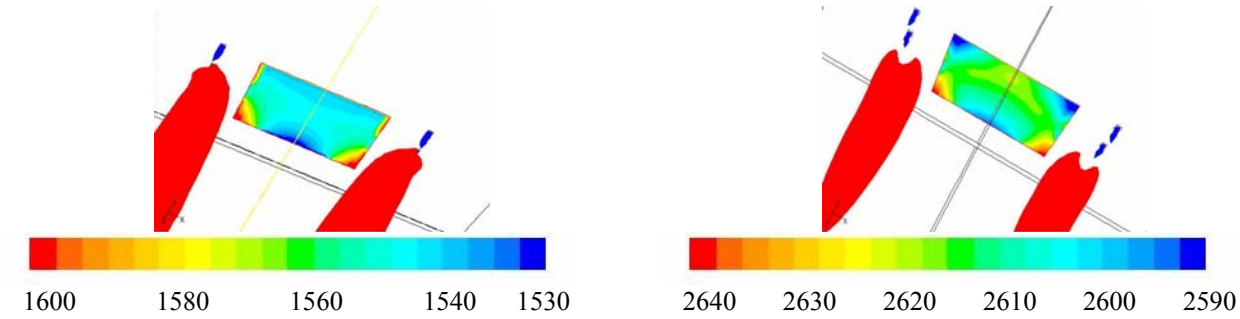

(a) natural gas (b) pentane

Figure 10 – Flames and temperature distribution at the chimney.

3.2. Species distribution

The methane (CH_4) is the most abundant component in the natural gas, representing 70% of its mass composition. Therefore, the analysis of this species gives a good idea of how the fuel is consumed inside the furnace. Comparison of the results for the pentane and methane are shown in Fig. 11. Figure 12 illustrates the isosurfaces of 3% of oxygen for both cases. Analyzing these figures, it is observed that the concentration surfaces of fuels and oxygen shows the same pattern observed for the temperature. These isosurfaces also give a good idea of how the flame distributes itself along the furnace. The flame region is understood to be the region where the highest consumption of fuel occurs, followed by a great heat release and temperature raise. Once again, it can be concluded that the combustion of pentane occurs faster, closer to the entrance.

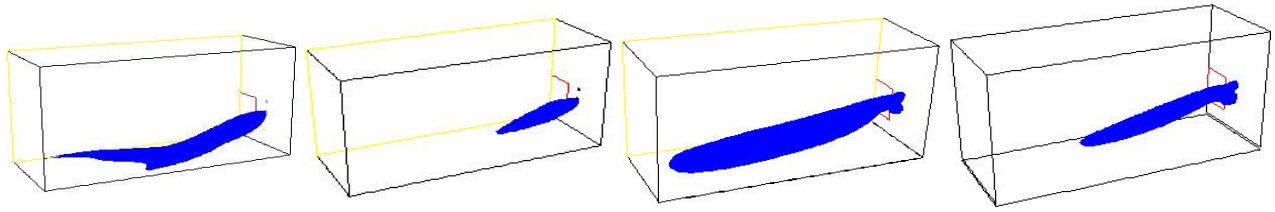

(a) natural gas (b) pentane

Figure 11– Isosurfaces of 1% fuel

(a) natural gas (b) pentane

Figure 12– Isosurfaces of 3% oxygen

Figure 13 shows profiles of oxygen mass fractions along lines inside the furnace: the *x* variation along a line passing through the center of the burner (y = 0.65m and z = 0.25m), and another one located 0.75 m away in the z direction (y = 0.65m and z = 0.90m). The peaks associated to *x* coordinates slightly below 0.80m indicates that the flames are aligned with the oxygen jets, and it is gradually consumed as *z* increases.

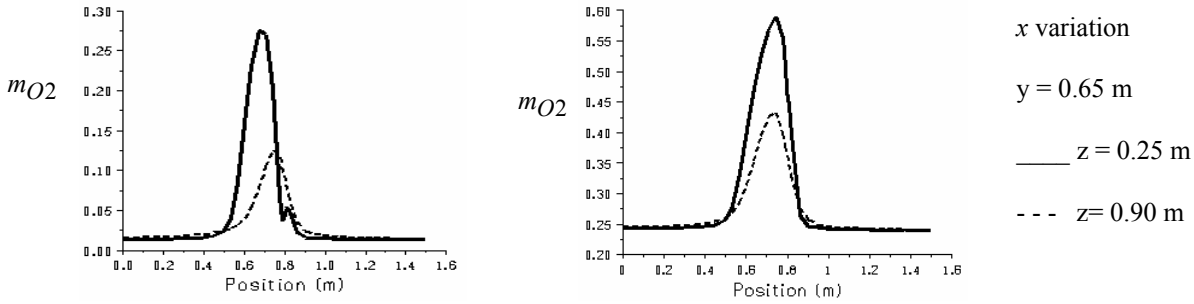

(a) natural gas (b) pentane

Figure 13 – Oxygen mass fraction profiles along lines inside the furnace.

The reactions of both natural gas and pentane create carbon dioxide, which is shown in Fig. 14, at several *x*-*y* plane along the *z* axial coordinate. The level of CO_2 is slightly higher for the natural gas. The lower concentration region corresponds to the region, where as already seen, the reactants are still present.

Figure 15 shows two views of the water distribution over the aluminum surface. High water concentration is not desirable because an aluminum oxide layer can be formed as water reacts with the surface of the load, which increases the thermal resistance and compromises the quality of the product. It is interesting to observe that the highest water concentration is under the flame for the pentane, but at the same region for the natural, one can find the lowest values. Note however, that the water distribution is almost uniform in both cases, with slightly higher value for the natural gas.

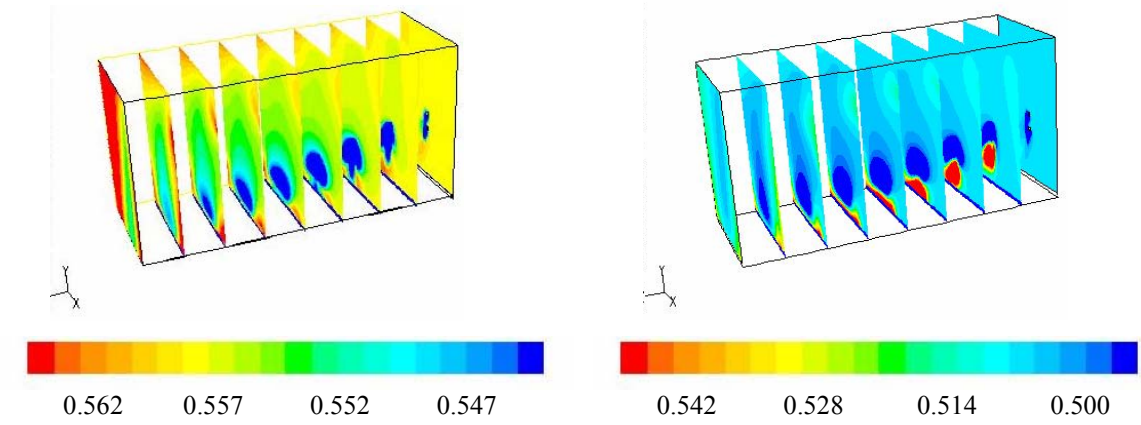

(a) natural gas (b) pentane

Figure 14 – Carbon Dioxide mass fraction inside the furnace.

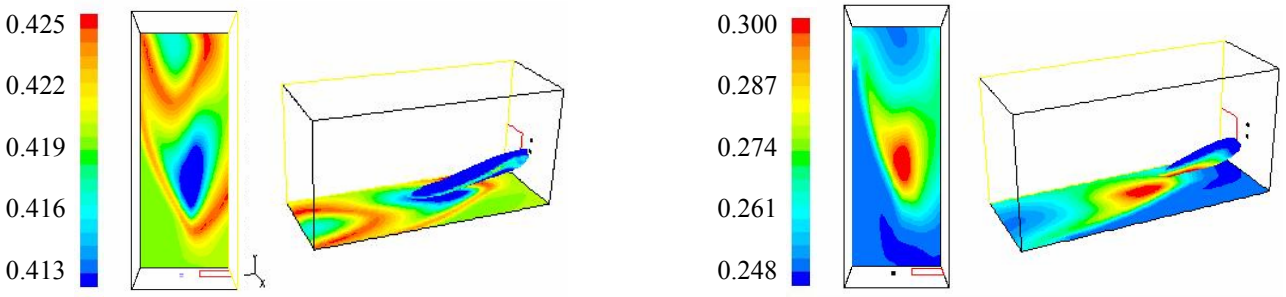

a) natural gas (b) pentane

Figure 15 – Water mass fraction distribution on the aluminum surface.

4. Conclusion

The numerical simulation of the process inside an aluminum melting furnace proved to be a helpful tool, which can contribute to improve several aspects of industrial interest, for example, reduction of material costs on maintenance of the refractory walls, increase of the efficiency of the fusion process, assurance of the quality of the product by the investigation of the deposition of water on the aluminum surface, better positioning of the burner and oxygen injectors, etc.

The numerical simulation also allows the easy investigation of the influence of several variables on the process; however, the mathematical models that will be used must be carefully chosen to maximize reliability on the results, not bringing unreal physical situations representing the phenomena.

The choice of the type of fuel used as energy source for the aluminum fusion can be crucial to achieve better efficiency on the process. In this way, the option for a liquid or gaseous fuel can significantly alter the combustion aspects inside the furnace, such as the formation of too long or too intense flames, leading to hot spots on the refractory walls and a non uniform heat flux distribution on the aluminum load.

Although a direct numerical comparison with experimental results was not performed due to lack of experimental data, the turbulence and combustion model employed here was used to predict the flow characteristics in the industrial aluminum remelting reverb furnace (Nieckele et al., 2004) with reasonable results.

The present analysis showed that it is possible to substitute the liquid fuel by natural gas. Although a longer flame was obtained for the natural, lower temperature level at the refractory walls is a positive factor for the substitution, as well as a more uniform heat flux at the aluminum surface.

5. Acknowledgement

The authors thank CNPq, Finep, Petrobras and ANP for the support during the development of this work.

6. References

Brewster, B.S.; Webb, B.W.; McQuay; M.Q.,D'Agostini, M. and Baukal, C.E., 2001, "Combustion Measurements And Modelling In An Oxygen-Enriched Aluminium-Recycling Furnace," J. of the Institute of Energy, **74**, pp. 11-17.

Correa, S. M. Shyy, W.,1987, "Computational Models And Methods For Continuous Gaseous Turbulent Combustion", Prog. Energy Combustion. Sci., v. 13, p. 249-292.

Christo, F.C., Fletcher, D.F. e Joseph, J.D., 1998, "Computational Fluid Dynamics Modelling Of A Landfill Gas Flare", J. of the Institute of Energy, v. 71, n.488, p.145-151.

Desjardin, P.E. and Frankel, S.H., 1996, "Assessment Of Turbulent Combustion Submodels Using The Linear Eddy Model", Combustion and Flame, v104, p. 343-357.

Eaton, A.M., Smoot, L.D. and Eatough, C.N., 1999,, "Components, Formulations, Solutions, Evaluation, And Application Of Comprehensive Combustion Models", Progress in energy and combustion science, v 25 n 4 p. 387-436.

Fluent User's Guide, v. 4.3,1995, Fluent Inc., New Hampshire.

Gomes, M. S. P., Nieckele, A.O., Naccache, M. F., and Kobayashi, W., 1997, "Numerical Investigation of the Oxygen Enriched Combustion Process in a Cylindrical Furnace", Proc. 4th Int. Conf. on Tech. and Combustion for a Clean Environment, Portugal, vol. II, Oxy-combustion, 36.1, pp. 1-5.

Goldin, G. M. and Menon, S.A. 1998, "Comparison of Scalar PDF Turbulent Combustion Models", Combustion and Flame, v 113 n 3 p. 442-453.

Gorner, K. e Zinser, W., 1990, "Simulation Of Industrial Combustion Systems", Int. Chem. Eng., v. 30, n. 4, p. 607-619.

Gran, I.R. and Magnussen, B. F., 1996, "A Numerical Study Of A Bluff-Body Stabilized Diffusion Flame - Part 2 - Influence Of Combustion Modeling And Finite-Rate Chemistry", Combust. Sci. and Tech., v.119, p. 191-217.

Gran, I.R., Ertesvâg, I.S. and Magnussen, B. F., 1997, "Influence of Turbulence Modeling on Predictions of Turbulent Combustion", AIAA Journal, vol 35, no. 1, p. 106-110.

Jones, W.P.; Sheen, D.-H.; 2000, "A Probability Density Function for Modeling Liquid Fuel Sprays", Journals of Flow, Turbulence and Combustion, vol. 63, no.1/4, pp. 379-394 (16)

Kuo, K.K., 1986. Principles of Combustion, John Wiley & Sons, New York.

Launder, B.E. and Spalding, D.B., 1974. "The Numerical Computation of Turbulent Flows", Computer Methods in App. Mech. and Engineering, 3, p. 269-289.

Ma, C.Y., Mahmud, T., Gaskell, P.H. and Hampartsoumian, E., 1999, Proc. of the Institution of Mechanical Engineers, Journal of Mechanical Engineering Science, Part C, v. 213, n.7, p. 697-705.

Magel, H.C., Schnell, U., and Hein, K.R.G., 1996, "Modeling Of Hydrocarbon And Nitrogen Chemistry In Turbulent Combustor Flows Using Detailed Reaction Mechanisms", 3rd Workshop on Mod. of Chem. Reac. Systems, Heidelberg.

Mukhopadhyay, A.; Puri, I.K.; Zelepouga, S. and Rue, D.M., 2001, "Numerical Simulation of Methane-Air Nozzle Burners for Aluminum Remelt Furnaces," 2001 ASME-IMECE, USA, CD-ROM, HTD-24234.

Nieckele, A.O.; Naccache, M. F.; Gomes, M. S. P. and Kobayashi, W., 1998, "Numerical Investigation of The Staged Versus Non-Staged Combustion Process in an Aluminum Melting Furnace," 1998 AIAA/ASME Joint Thermophysics and Heat Transfer Conf., USA, **1**, pp. 253-259.

Nieckele, A.O.; Naccache, M. F.; Gomes, M. S. P. and Kobayashi, W., 1999, "The Influence Of Oxygen Injection Configuration In The Performance Of An Aluminum Melting Furnace," 1999 ASME-IMECE, USA, Heat Transfer Division, **2**, pp. 405-412.

Nieckele, A.O.; Naccache, M.F.; Gomes, M. S. P.; Carneiro, J.N.E.; Serfaty, R., 2002, "Numerical Simulation of Natural Gas Combustion Using a One Step and a Two Step Reaction", 2002 Asme Imece, International Conference of Mechanical Engineering, November 11-16, New Orleans, LO, USA

Nieckele, A.O., Naccache, M. F., Patankar, Gomes, M. S. P., 2004, "Numerical Simulation of a Three Dimensional Aluminum Melting Furnace", Journal of Energy Resources Technology, ASME, vol. 126, pp.72-81.

Patankar, S.V. and Spalding, D.B., 1967. Heat and Mass transfer in Boundary Layers, Morgan-Grampian, London.

Reveillon, J.; Vervisch L.; 2000, "Spray Vaporization in Nonpremixed Turbulent Combustion Modeling: a Single Droplet Model", Journals of Combustion and Flame, April 2000, vol. 121, no. 1, pp. 75-90 (16).

Siegel, R. and Howell, J.R., 1981. Thermal Radiation Heat Transfer, 2nd edition, Hemisphere Pub. Corp., New York.

Sivathann, Y.R. and Faeth, G.M, 1990, "Generalized State Relationships for Scalar Properties in Non Premixed Hydrocarbon/Air Flames, Combustion Flame, v. 82, p.211-230.

Smith, T.F., Shen, Z.F., and Friedman, J.N., 1982. "Evaluation of Coefficients for the Weighted Sum of Gray Gases Model", Transactions of the ASME - Journal of Heat Transfer, v. 104, p. 602-608.

Zimont, V., Polifke, W. and Bettelini, M., 1998, "An Efficient Computational Model For Premixed Turbulent Combustion At High Reynolds Numbers Based On A Turbulent Flame Speed Closure", Journal of Engineering for Gas Turbines and Power, v. 120, n.3, p.526-532.

7. Copyright Notice